Yeast-Derived Carbon Nanotube Coated Separator for High Performance Lithium-Sulfur Batteries

Jiajun He, Zan Gao, Xiaodong Li*

Department of Mechanical and Aerospace Engineering

University of Virginia

122 Engineer's Way

Charlottesville, VA 22904-4746 (USA)

*Corresponding author. E-mail: xl3p@virginia.edu, Tel: 434-243-7762

Abstract

Lithium-sulfur (Li-S) battery is an appealing energy storage technology because of its

superior theoretical energy density, natural friendliness, and low cost over Li-ion battery. However,

Li-S batteries often suffer from fast capacity decay, low energy density, and short lifespan due to

the shuttle effect from polysulfides. Hybridizing sulfur with carbonaceous materials has been

demonstrated effective in solving these challenges and thus improving Li-S battery performance.

In this work, yeast as a low-cost, natural, and renewable catalyst was used to grow carbon

nanotubes (CNTs), which were then coated on the separator in a Li-S battery to suppress the shuttle

effect of polysulfides. The Li-S cell with the CNT coated separator exhibited significantly

improved performance at high current density with an initial high specific capacity of 980 mA h

g⁻¹ and a well-retained specific capacity of ~450 mA h g⁻¹after 850 cycles at a high current density.

Keywords: Carbon nanotube, yeast, lithium-sulfur battery, biomass

1 Introduction

Continuous consumption of nonrenewable energy resources accompanied by ever-increasing environmental issues calls for rapid development of advanced energy storage systems that utilize renewable energy resources.[1-3] However, one stern reality is that conventional lithium-ion batteries, which are currently the predominant energy storage devices, have almost reached their theoretical limit.[4-6] In this context, the lithium-sulfur (Li-S) battery has attracted special attentions as a promising next-generation energy storage technique due to its theoretically ultrahigh specific capacity (1675 mA h g⁻¹) and energy density (2600 W h kg⁻¹).[7] Nonetheless, Li-S batteries have not fully filled their promise because there are multiple challenges on the road to practical application such as the insulating nature of sulfur, the dissolution of lithium polysulfides, and the volume change of cathode during cycling, jointly leading to drastic capacity decay and severe self-discharge and thus shortening battery's lifespans.[8]

Various design strategies have been explored to mitigate the aforementioned problems to enhance the performance of Li-S battery. Advanced carbon materials, such as porous carbons, graphene, and carbon nanotubes (CNTs), have been used to construct Li-S battery cathodes and separators.[9-14] CNTs have been served as the sulfur host for sulfur encapsulation due to CNTs' superior electrical conductivity and porous/tubular structural features that improve the electrode conductivity and retard the shuttle effect of soluble polysulfides.[15-21] Additionally, CNTs were used as an interlayer between the cathode and the separator.[22-24] Inserting an interlayer was found to be more efficient in suppressing the dissolution of polysulfides than adding carbon materials into the cathode.[25-30] Although CNTs have been proven to be beneficial to enhancing Li-S battery performance, they are still costly due to low production rate of CNTs.[31-34] Chemical vapor deposition (CVD) is the predominant CNT fabrication method.[35-37] During the

CVD process, hydrocarbons, such as methane and acetylene, are converted into CNTs with the aid of metallic catalyst nanoparticles.[38] The high cost of CVD fabrication comes from the harsh reaction conditions, expensive catalysts, and complicated post-purification processes.[39-42] Furthermore, the CVD method may further exacerbate the energy crisis as the broadly used hydrocarbons are mainly derived from nonrenewable fossil fuels.[43, 44] Therefore, an important question emerges: is there a sustainable and cost-effective process to produce high-quality CNTs for Li-S battery application?

Nature renders infinite possibilities. Biomass materials, which are rich in carbon and gifted with incredible structures and properties, are highly promising for fabricating advanced carbon materials which find to be forceful for enhancing Li-S battery performance. For example, camphor was used as a raw material to grow CNTs.[45] Cotton textile and recycled paper were used to modify the cathode and separator of Li-S battery, .[46-49] Recently, we demonstrated that yeast, a renewable unicellular fungus that is widely used in baking and ethanol industries, can work with flour to grow CNTs.[50] The fermented flour was carbonized and converted into an activated wheat flour dough/carbon nanotube (AWD/CNT) composite, which was then used as the sulfur host for Li-S battery cathode. Yeast was found to be a possible bio-catalyst for synthesizing CNTs. Moreover, its low cost and natural abundance enable CNT production cost-effective and sustainable. However, application of the fermented flour-derived CNTs in Li-S battery is limited by the introduction of impurities, the carbonized wheat flour, which would negatively affect the Li-S battery performance. On the other hand, yeast has been demonstrated as a feasible biotemplate to produce porous carbon for enhancing Li-S battery performance. [51, 52] Therefore, we propose to activate yeast to form porous carbon scaffold and simultaneously grow CNTs on the scaffold with yeast as a catalyst for Li-S battery application.

In this work, yeast's catalytic function on CNT growth was further validated by combining yeast with various carbon sources for growing CNT. High-quality CNTs were directly grown on activated yeast (AY) scaffold with yeast as the catalyst and cotton as the carbon source. Such AY/CNT composite powders with the ultrahigh specific surface area were then coated onto the cathode side of the separator in Li-S battery to strengthen the function of Li-S battery separator. The AY/CNT modified separator rendered significantly improved specific capacity and cyclic stability of ~450 mA h/g after 850 cycles at a high current density.

2 Material and Method

2.1 Preparation of AY/CNT composite powders

The yeast used in the experiment was directly purchased from grocery store. Typically, 2.5 g yeast (Zhenhaojia Yeast) was fermented in 100 ml deionized water (DI water) at 30 °C for 3 h. After stirring, the solution was frozen and dried by a vacuum freeze dryer (Columbia International). The freeze-dried fermented yeast was then ground into powders and stored at 0 °C for future use. 0.25 g of such fermented yeast was placed in a stainless steel crucible (20 mm × 12 mm × 6 mm). The crucible was then wrapped with a piece of cotton textile (80 mm × 50 mm) and placed into a tube furnace (Thermolyne 21100), held at 750 °C for 2 h under a 200 sccm argon flow to synthesize the AY/CNT composite which afterwards was collected, washed by DI water and then dried at 80 °C.

2.2 Verification of the catalytic function of yeast for CNT growth

In the aforementioned synthesis of CNTs, yeast was used as the catalyst while cotton as the carbon source. Can yeast catalyze the CNTs growth when alternative carbon sources are used?

Here a piece of recycled cardboard (1 cm × 5 cm) and a segment of corn cob with a length of 1 cm were applied as two biomass carbon source alternatives to cotton. They were respectively dipped in 100 ml yeast solution (2.5% wt), dried at 80 °C for 4 h and then held at 750 °C for 2 h under a 200 sccm argon flow.

2.3 Coating AY/CNT composite powders onto the Li-S battery separator

The AY/CNT composite powders were coated onto the separator (Celgard 2400 film) via a slurry coating method. A mixture of the composite particles and the binder -polyvinylidene fluoride (PVDF) with a mass ratio of 9:1 was ground in N-methylpyrrolidone (NMP) to form a slurry, which was then scrapped onto one side of the conventional separator to form a 50 µm thick coating of AY/CNT. The AY/CNT coated separator was then dried in an oven at 60 °C for 24 h. The dried separator was punched into disks of a diameter of 1.7 cm.

2.4 Cathode preparation

Cathodes were prepared with a slurry coating consisting of sulfur powder, carbon black, and PVDF in a ratio of 7:2:1, which were dispersed in NMP to form the slurry. The slurry of a thickness of 150 µm was then scrapped onto an aluminum foil. After being dried at 60 °C for 12 h, the coated aluminum foil was punched into disks of a diameter of 1.2 cm as the cathodes for coin cells. The cathode sulfur loading was measured to be 2.5 mg/cm².

2.5 Electrochemical efficacy of AY/CNT coated separator

The CR2032 type coin cells were assembled with the modified AY/CNT separator and the pristine Celgard separator respectively to evaluate the electrochemical efficacy of the AY/CNT

coated separator. The cells were assembled in an argon-filled glove box (Mbraun) with the mentioned cathodes, separators and electrolyte (1 M lithium bis(trifluoromethane sulfonyl)imide (LITFSI) and 0.2 M LiNO₃ in 1:1 v/v 1, 2-dimethoxyethane (DME) and 1, 3-dioxolane (DOL) solution). The cell with the AY/CNT coated separator facing the cathode was annotated as the AY/CNT cell, and the cell with a pristine separator (no AY/CNT coating) was labeled as the reference cell. The cells were tested at voltages ranging from 1.7 V to 2.8 V with a LAND CT battery tester. Additionally, a CHI 660 electrochemical workstation was used to measure the cyclic voltammetry (CV) characteristics at a scan rate of 0.0001 V/s and the electrochemical impedance spectroscopy (EIS) values at the frequency ranging from 0.01 Hz to 100000 Hz and an AC voltage amplitude of 0.005 V.

2.6 Materials characterization

The specific surface areas of activated yeast and AY/CNT powders were measured using a Quantachrome Autosorb iQ nitrogen adsorption/desorption analyzer based on the Brunauer-Emmett-Teller (BET) theory. Scanning electron microscopy (SEM; FEG 650 with energy dispersive spectroscopy), high-resolution transmission electron microscopy (HRTEM; FEI Titan), X-ray diffraction (XRD; PANalytical X' Pert Pro Multi-purpose diffractometer equipped with Cu K_{α} radiation with $\lambda = 0.015406$ nm), Raman spectroscopy (Renishaw Invia Raman microscope with the laser at 514 nm), and X-ray photoelectron spectroscopy (XPS; PHI Versa-Probe III) were used to characterize the microstructure and compositions of materials and cells used in this study.

3. Results and Discussion

As shown in Fig. 1a, the crucible filled with yeast was wrapped by a piece of cotton textile without physical contact between the yeast and the cotton. Here, cotton served as the carbon source for CNT growth during the carbonization process through a vapor-liquid-solid (VLS) mechanism. Specifically, during the heat treatment, cotton textile was decomposed and released various gaseous hydrocarbons such as acetone, ethanol and methane (Fig. 1b), which would further be decomposed into carbon and eventually precipitated on the surface of the yeast.[53] Attributed to the catalytic function of yeast, the precipitated carbon particles grew into CNTs (Fig. 1c). SEM inspection (Fig. 1d) reveals a large number of CNTs produced on the activated yeast particles, whereas no CNTs were found on the activated cotton textile. This comparison suggests that yeast was the catalyst for the growth of CNTs and cotton only served as carbon source since CNTs were only observed on yeast, not on cotton. For further demonstration, cotton and fermented yeast were heated respectively under the same condition, which turned out that no CNTs were observed on either of them (Fig. 1e, 1f). The failure of growing CNTs on cotton was due to the lack of catalysts, while the absence of CNTs on AY particles was ascribed to the lack of carbon source. The loading of CNTs on the AY particles was estimated to be ~9450 CNTs per AY particle based on ten randomly selected AY/CNT particles. The specific surface area of AY/CNT was measured to be $220.192 \text{ m}^2/\text{g}$, three times more than that of the bare AY particles (67.001 m²/g), which resulted from tubular CNTs on the AY/CNT composite (Fig. S-1). HRTEM inspection (Fig. 1h) shows a curved CNT with a length of over 2 µm, a diameter of ~30 nm and a wall thickness of ~10 nm (Fig. 1i). FFT (inset of Fig. 1i), XRD and Raman spectroscopy (Fig. S-2) inspections jointly reveal that the CNTs are of amorphous phase. The similar intensities of the D band (~1350 cm⁻¹) and the

G band (~1580 cm⁻¹) in the Raman spectrum indicate high quantities of defects in the AY/CNT composite powders.[54]

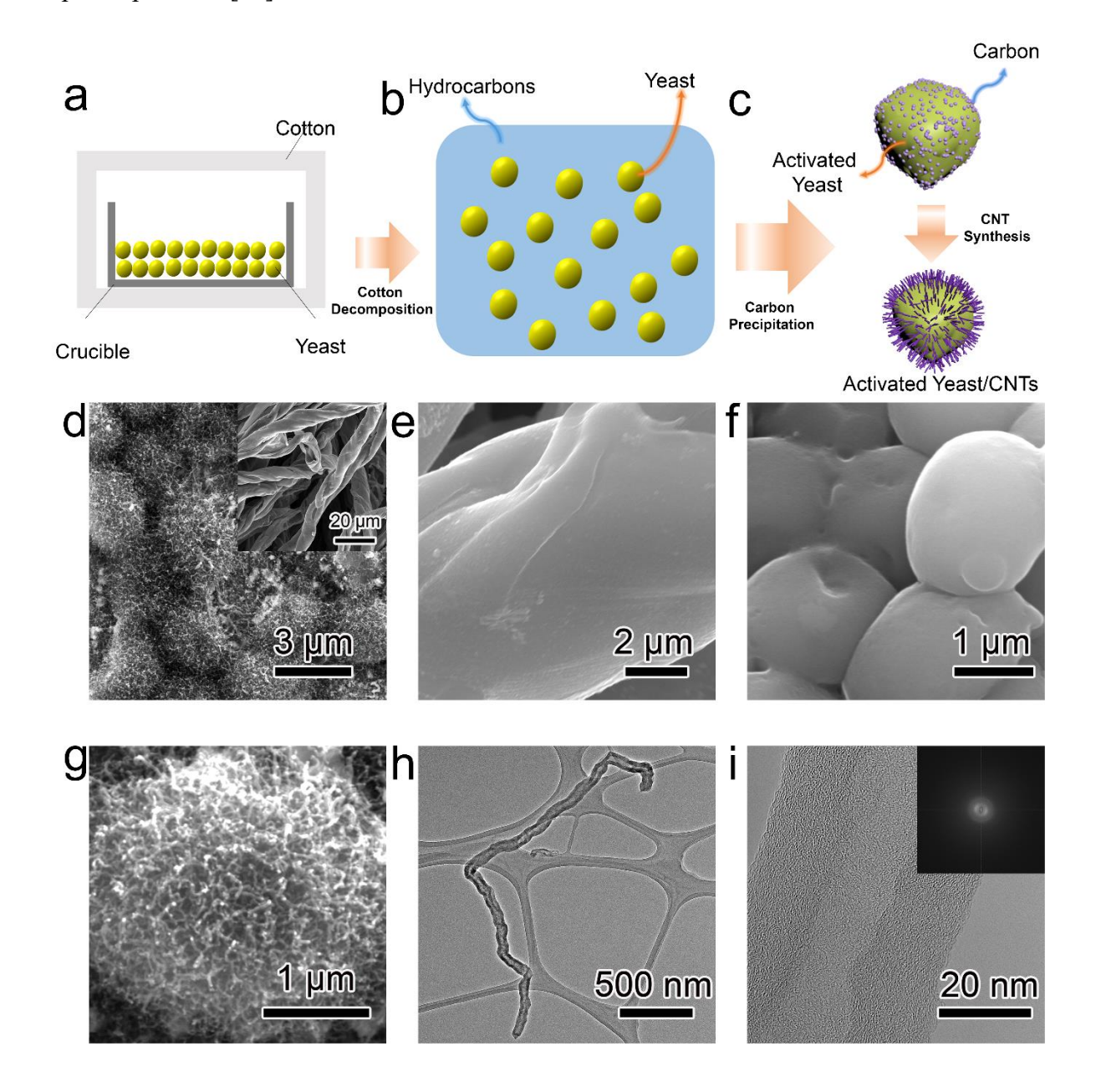


Fig. 1. Characterization of the AY/CNTs composite. (a − c) Schematics that display the process of CNT growth: A crucible containing yeast wrapped by cotton (a); the decomposition of cotton and release of hydrocarbons (b); carbon precipitation and CNT growth on yeast surface (c); (d) SEM images of the AY/CNT composite, inset shows activated cotton textile (ACT); (e) and (f)

SEM images of ACT and AY; (g) SEM image of an AY/CNT particle; (h) TEM image of a CNT derived from yeast; (i) HRTEM image of the CNT derived from yeast, inset shows the corresponding FFT pattern.

Apparently, the fermented yeast acted as the catalyst for CNT growth. An important question is: which chemicals catalyze the growth of CNTs? Energy dispersive spectroscopy (EDS) imaging observed four main elements, C, O, P, and K, in the AY/CNT composite (Fig. S-3). Among them, potassium is a very active metallic element that can easily form compounds with other elements. The broad peaks in the XRD spectrum indicate the existence of potassium salts such as potassium carbonate and potassium phosphate. Potassium salts have been previously reported to have catalytic functions for CNT growth.[55, 56] It is persuasive that these potassium salts formed during the heat treatment worked as the catalysts for CNT synthesis (Fig. 2a).

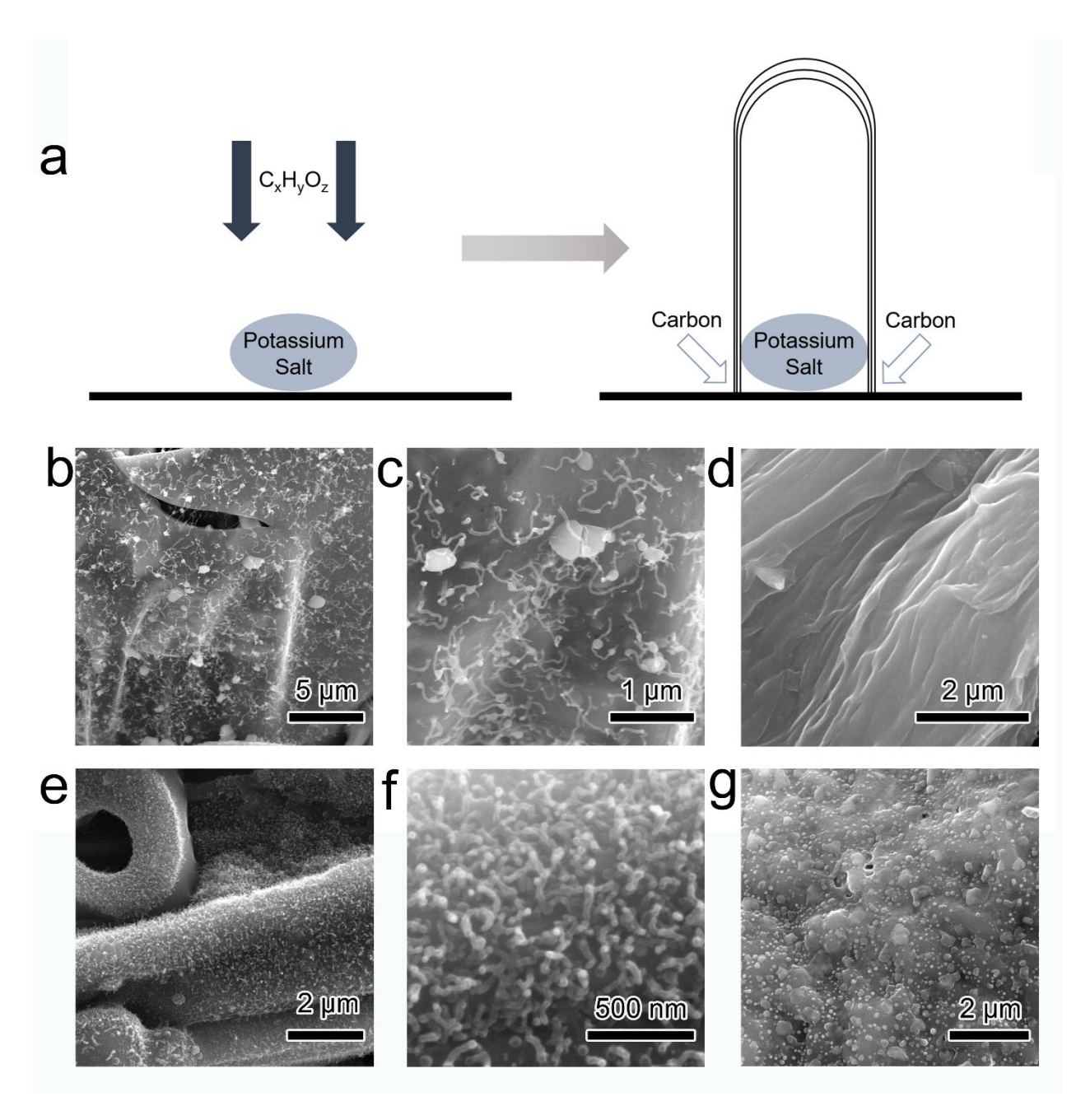


Fig. 2. Yeast's catalytic function for CNT synthesis. (a) Schematics of CNT growth enabled by the potassium salts derived from fermented yeast; (b) and (c) SEM images of CNTs grown on the recycled cardboard precursor; (d) SEM image of carbonized cardboard (without being dipped in yeast solution); (e) and (f) SEM images of CNTs grown on the corn cob precursor; (g) SEM image of carbonized corn cob (without being dipped in yeast solution).

With yeast's catalytic function being demonstrated, more biomass materials were used as carbon sources to validate yeast's catalytic capability for CNT growth. Recycled cardboard and corncob, two different types of biomass materials, were dipped in the yeast solution and dried at 80 °C for 4 h and then heated at 750 °C for 2 h under a 200 sccm argon flow for yeast-catalyzed CNT synthesis. SEM inspection shows that CNTs were synthesized with both biomass carbon precursors (Fig. 2b, 2c, 2e, 2f). More CNTs were found on the corncob surface than the recycled cardboard surface (Fig. 2d, 2g), indicating that the corncob provided more carbon than the recycled cardboard. For comparison, the recycled cardboard and corncob were heated individually without being dipped in the yeast solution, and CNTs cannot be observed on either of them. All results illustrate that yeast is indispensable for CNT growth, no matter what biomass materials are used.

To apply the yeast-derived CNTs to Li-S batteries, the AY/CNT powders mixed with polyvinylidene fluoride (PVDF) were coated onto the cathode side of the separator (Fig. 3a). The cross-sectional image of the coated separator illustrated that the coating layer was diffused into the separator and the total thickness was ~50 μm. As the thickness of the pure separator was 30 μm, the height of the AY/CNT coating layer was measured as 20 μm. The XPS and EDS analyses of AY/CNT coating show that in addition to fluorine from the PVDF (Fig. 3c, Fig. S-3), ester groups, which have strong bindings with polysulfide,[57] were observed on the coating and expected to block the flow of polysulfides from the cathode to the anode during Li-S battery cycling.

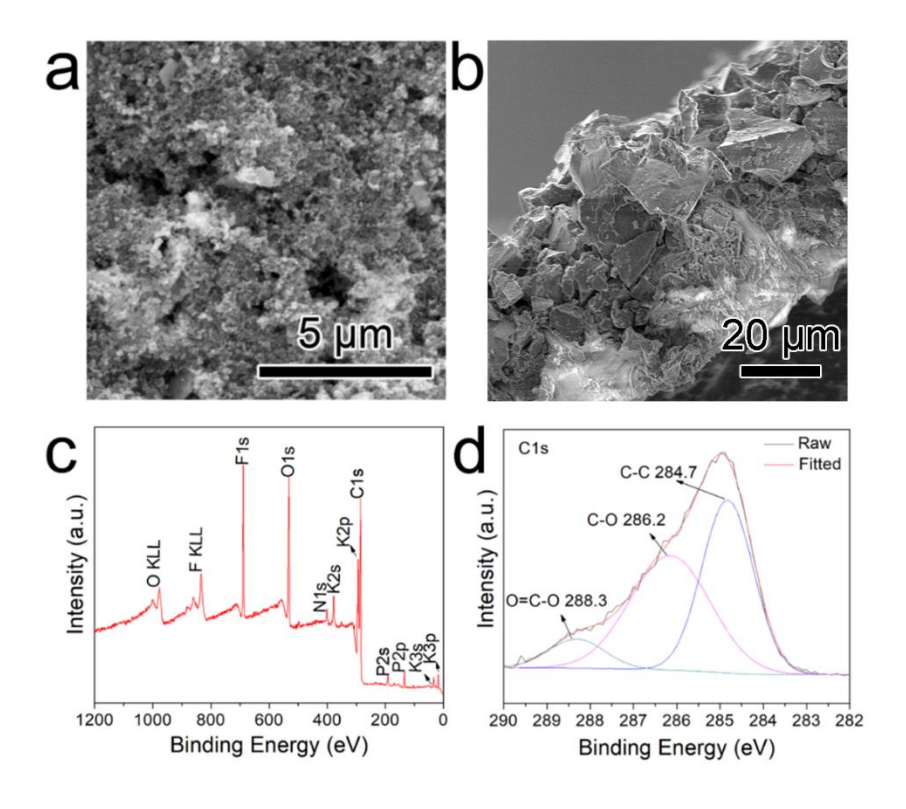


Fig. 3. Characterization of the AY/CNT coating on the Li-S battery separator before battery cycling. (a) and (b) SEM images of the top and cross-sectional views of the AY/CNT coating; (c) Survey spectrum of the AY/CNT coating; (d) C1s spectrum of the AY/CNT coating.

The efficacy of the AY/CNT coating was examined by comparing the electrochemical performances of the Li-S batteries with and without the AY/CNT coating on the separators. As shown in Fig. 4a, the CV curve of the reference battery without the AY/CNT coating on the separator shows a charging peak at ~2.5 V and one discharging peak at ~2.2 V. As for the coating battery, the discharging plateau was broader with the peak at ~2.1 V, and the charging reaction was illustrated as a curve from 1.7 V to 2.8 V without obvious charging plateau. The change on the CV curve was attributed to the AY/CNT coating layer. The localized rates of Li₂S/Li₂S₂ to S₈ were different because of the non-uniformity of CNT distribution on the coating layer, which

suppressed the charging plateau. The effects of the coating layer were also illustrated in the EIS spectrum (Fig. 4b), where a second semicircle was found at the middle-frequency region, and the line at the low-frequency region was extended. The second semicircle indicated the charge transfer of sulfur intermediates at the AY/CNT coating layer.[58] The line in the EIS curve was related to the formation of Li₂S/Li₂S₂, and the extension of the line after adding the coating layer corresponded to the broader discharging plateau (Fig. 4a). Although the resistance was increased by the coating layer, it still enhanced the initial specific capacity by ~200 mA h g⁻¹ at a current density of 0.24 mA/cm² (denoted as 1 C) as shown in the galvanostatic discharging curve (Fig. 4c). Further recording of the charging/discharging curves of the first four cycles of the battery with the AY/CNT coating on the separator exhibit ultra-high and stable discharging specific capacities of 1282.1, 1229.3, 1242.2, and 1253.5 mA h g⁻¹, respectively (Fig. 4d). The rate performance (Fig. 4c) showed that the AY/CNT coating enabled a specific capacity at ~1000 mA h g⁻¹ with the current density being increased to 4 C. The battery without the AY/CNT coating experienced a drastic capacity decay while the current density being doubled from 1 C to 2 C. At 4 C, this reference battery only possessed a specific capacity at ~300 mA h g⁻¹. The significant improvement of specific capacity, especially at the high current density, was attributed to suppression of shuttle effect and change of reaction rate enabled by the AY/CNT coating layer. Another pair of batteries with and without the AY/CNT coating was tested at 4 C for 200 cycles (Fig. 4e). In general, the reference battery experienced a capacity increase and kept stable at ~420 mA h g-1. As a comparison, the AY/CNT coating battery showed higher initial specific capacity, which was gradually decreased for 90 cycles, then increased and suddenly decayed at 160 cycles with a stable capacity of 650 mA h g⁻¹. The increase in specific capacity during battery cycling has been found in biomass-derived carbon anode Li-S batteries.[48, 59] The increase shown in the AY/CNT

battery from the 90th to 100th cycle was attributed to the utilization of lithium polysulfide in the coating layer. Further tests of the AY/CNT coating battery performance at a high current density was conducted and it also exhibited an increase in specific capacity from an initial specific capacity of 601 mA h g⁻¹ to 776.2 mA h g⁻¹ at the 200th cycle at a current density of 10 C (Fig. 4f). At such a high specific capacity, the Coulombic efficiency remained ~90%. When the current density dropped down to 5 C, the Coulombic efficiency retained a record high of 98% while the specific capacity recovered to ~980 mA h g⁻¹ and then dropped down to ~ 450 mA h g⁻¹ at the 850th cycle. All the electrochemical results demonstrated that the incredible effect of the AY/CNT coating layer on suppressing "shuttle effect", which enabled the improved performance of Li-S battery with higher specific capacity and longer lifespan while sacrificing the conductivity to some extent.

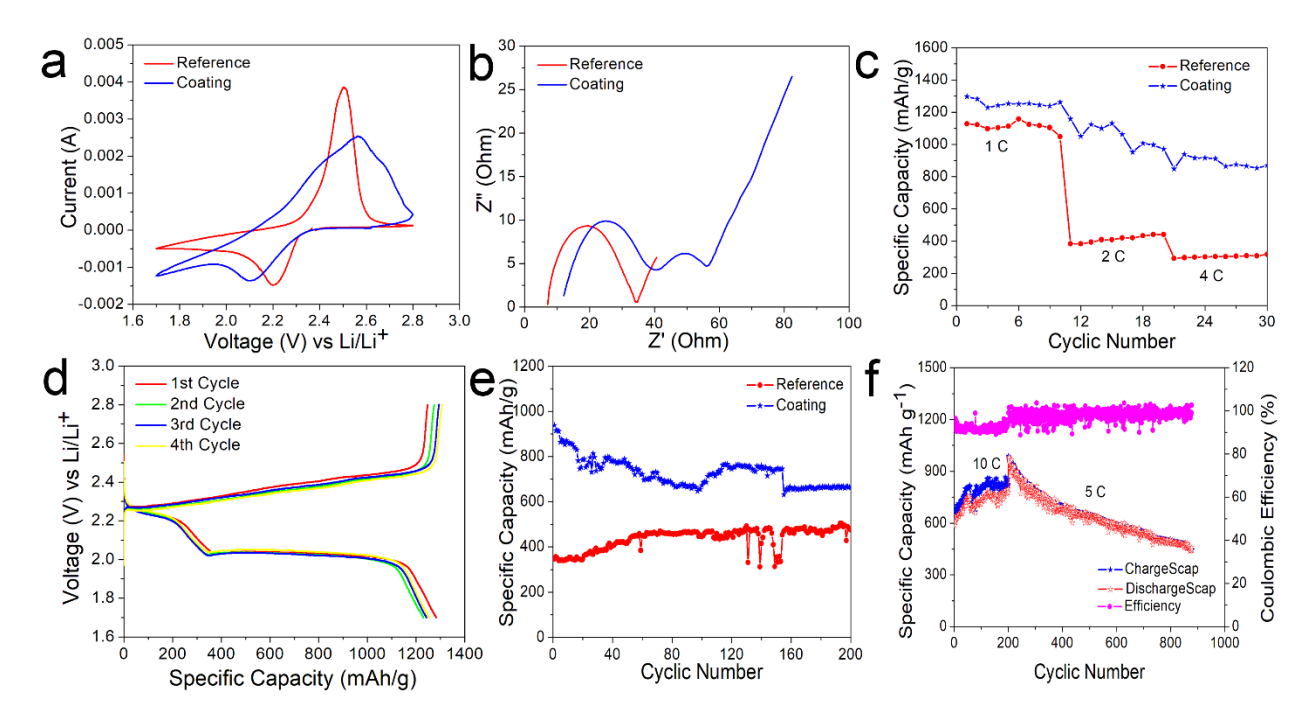


Fig. 4. Electrochemical characterization of the Li-S batteries with and without the AY/CNT coating. (a) Cyclic Voltammetry (CV) curves of the batteries; (b) Electrochemical impedance spectroscopy curves of the batteries at the 1st cycle; (c) Rate performance comparison of the batteries at 1 C, 2 C and 4 C; (d) The first four cycles of the charging/discharging curves of the

battery with the AY/CNT coating on the separator at 1 C; (e) Cyclic performance comparison; (f) Cyclic performance and corresponding Coulombic efficiency of the battery with the AY/CNT coating on the separator.

The enhanced electrochemical performance was attributed to the AY/CNT coating on the separator that encapsulated sulfur transportation during the battery cycling. The comparison of the anodes from the batteries with and without the AY/CNT coating exhibited that the anode from the fully discharged reference battery was covered by a layer of yellow particles, whereas no noticeable change was observed on the lithium foil from the cell with the AY/CNT coating (Fig. S-4). EDS mapping (Fig. S-5) revealed a large number of polysulfides (26.0% of S) on the anode of the reference battery, but fewer polysulfide particles (9.8% S) on that of the AY/CNT coating constructed battery (Fig. S-6a). Meanwhile, the AY/CNT coated separator captured 12.3% S (Fig. S-7), demonstrating the capability of trapping polysulfides during cycling. As for the reference battery, its separator was also analyzed by EDS mapping. Both sides of the separator were observed, and it could be seen that the ratio of sulfur on the cathode side reached 35.8%, while that on the anode side was 30.9% (Fig. S-8). The high and similar S ratio on both sides of the reference battery separator showed that the traditional separator does not show polysulfides trapping without the AY/CNT coating. XPS analysis (Fig. 5a) revealed two additional elements, Li and S, on the AY/CNT coating, as shown in Li 1s spectrum (Fig. 5b) and S 2p spectrum with three peaks at 163.02 eV, 165.57 eV, and 168.0 eV, respectively (Fig. 5c). The S 2p_{3/2} peak at 163.02eV indicates the deposition of polysulfide on the AY/CNT coating. The binding energy of S 2p_{3/2} is higher than that of pure sulfur, pointing toward the presence of C-S bonds. The most substantial peak at 168.0 eV should be attributed to the formation of sulfone between S and the

biomass-derived functional groups from the AY/CNT coating. Compared with that, the XPS spectrum of reference battery separator showed no sulfone on the surface, which could be explained by the absence of functional groups that could be connected with S (Fig. 5f). The effect of the functional groups from the AY/CNT coating also led to the difference in the Li 1s spectrum as Li was so active that connected to those functional groups (Fig 5b, Fig. 5e). On the other hand, the higher binding energy S 2p_{3/2} peak demonstrated the existence of C-S bonds, which came from the cathode with graphite/sulfur composite. Additionally, the Li 1s peak shown in Fig. 5e further proved the formation of polysulfides, and the formation of these bonds among S and other elements consumed the active materials, explaining the specific capacity decay during the first several cycles.

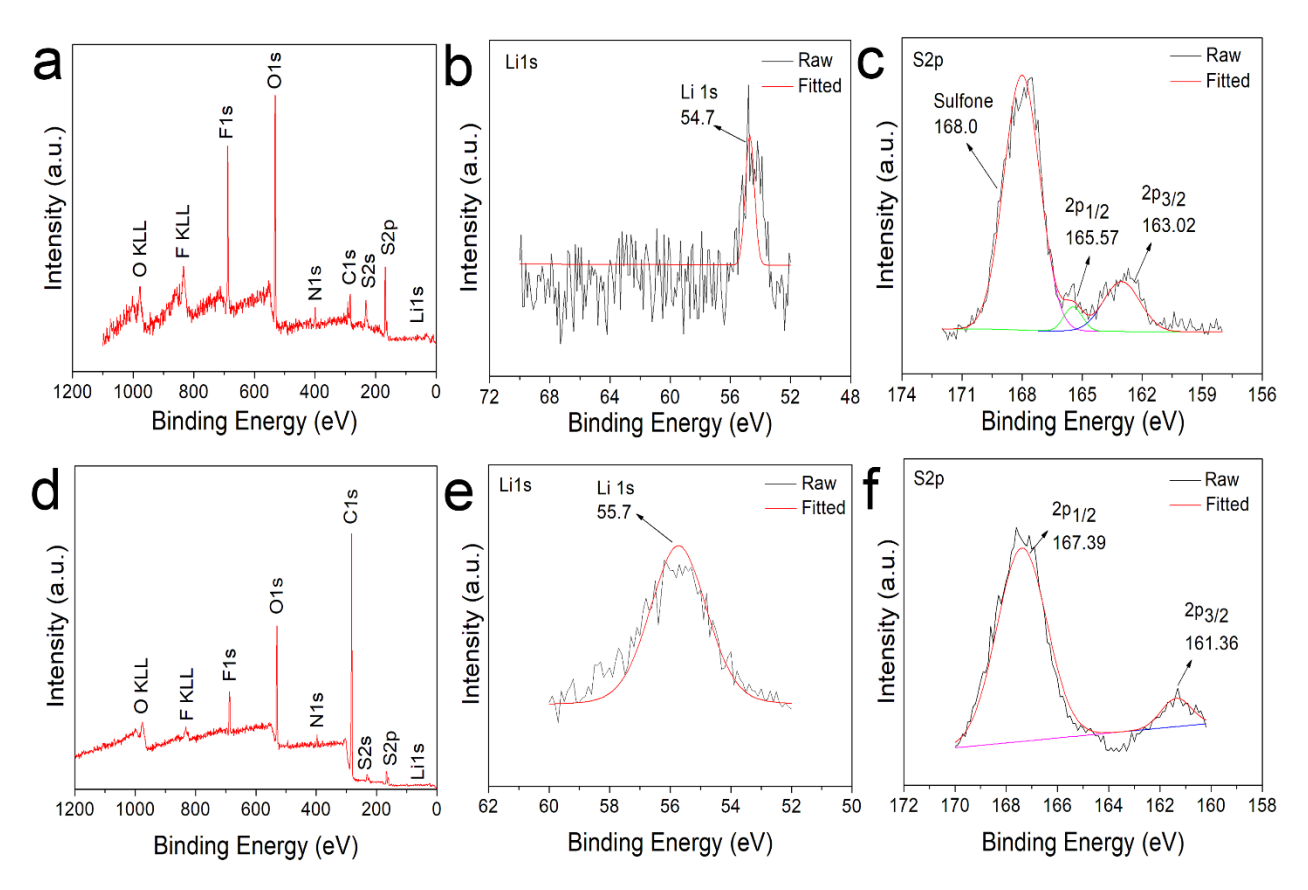


Fig. 5. XPS analysis of the AY/CNT coating from the AY/CNT coating battery and the traditional separator from the reference battery, respectively after the batteries were fully

discharged. (a) Survey spectrum of the AY/CNT coating; (b) Li1s spectrum of the AY/CNT coating; (c) S2p spectrum of the AY/CNT coating; (d) Survey spectrum of the separator; (e) Li1s spectrum of the separator; (f) S2p spectrum of the separator.

4. Conclusion

We investigated yeast's catalytic function for CNT growth by separating the carbon sources from yeast through wrapping yeast with a piece of cotton textile, and we found that CNTs directly grew on yeast particles. We have also successfully synthesized CNTs from fermented yeast by using different types of biomass materials as carbon sources, including recycled cardboard and corn cobs. The results jointly proved that yeast is a new type of biocatalyst for CNT growth. This new catalyst drastically reduces the cost of CNT manufacturing, especially when working with biomass carbon sources. Furthermore, the AY/CNT composite was used as an interlayer to modify the Li-S battery separator, significantly improving the performance of Li-S batteries. The yeast-derived CNT coated separator enabled a high specific capacity and long lifespan for its Li-S battery and should find more applications in next-generation energy storage systems.

Acknowledgments

Financial support for this study was provided by the U.S. National Science Foundation (CMMI-1728042). The authors thank the staff members at the University of Virginia NMCF for electron microscopy technical support.

Conflict of Interest

The authors declare no conflict of interest.

Appendix A Supplementary Data

BET analysis of carbonized yeast and AY/CNT composite, XRD and Raman Spectrum of AY/CNT composite, EDS maps of AY/CNT composite, Digital image of the lithium anodes from batteries with and without AY/CNT coating on the separator, EDS maps of lithium anodes and separator from batteries with and without AY/CNT coating on the separator.

References

- [1] M. Armand, J. M. Tarascon, *Nature*, 451, 652-657 (2008).
- [2] N. Armaroli, V. Balzani, Ener. & Enviro. Sci., 4, 3193-3222 (2011).
- [3] B. Dunn, H. Kamath, J. M. Tarascon, *Science*, 334, 928-935 (2011).
- [4] A. Aricò, P. Bruce, B. Scrosati, J. M. Tarascon, W. van Schalkwijk, *Nat. Mater.*, 4, 366–377(2005).
- [5] J. B. Goodenough, Y. Kim, Chem. Of. Mater., 22, 587-603 (2010).
- [6] X. Lou, C. Lin, Q. Luo, J. Zhao, B. Wang, J. Li, Q. Shao, X. Guo, N. Wang, Z. Guo, Chem. Electro. Chem. 4, 3171-3180 (2017).
- [7] Y. X. Yin, S. Xin, Y. G. Guo, L. J. Wan, Angew. Chem. Int. Edit., 52, 13186-13200 (2013).
- [8] P. G. Bruce, S. A. Freunberger, L. J. Hardwick, J. M. Tarascon, Nat. Mater., 11, 19-29(2012).
- [9] X. Ji, K. T. Lee, L. F. Nazar, *Nat. Mater.*, 8, 500-506 (2009).
- [10]Y. Zhang, Z. Gao, N. Song, J. He, X. Li, Mater. Today Ener., 9, 319-335 (2018).
- [11] J. Wang, S. Y. Chew, Z. W. Zhao, S. Ashraf, D. Wexler, J. Chen, S. H. Ng, S. L. Chou, H. K. Liu, *Carbon*, 46, 229-235 (2008).
- [12] J. Guo, Y. Xu, C. Wang, *Nano Lett.*, 11, 4288-4294 (2011).
- [13] M. Q. Zhao, X. F. Liu, Q. Zhang, G. L. Tian, J. Q. Huang, W. Zhu, F. Wei, ACS Nano, 6, 10759-10769 (2012).
- [14] H. J. Peng, J. Q. Huang, M. Q. Zhao, Q. Zhang, X. B. Cheng, X. Y. Liu, W. Z. Qian, F. Wei, Adv. Funct. Mater., 24, 2772-2781 (2014).
- [15] S. Iijima, *Nature*, 354, 56-58 (1991).
- [16] B. Peng, M. Locascio, P. Zapol, S. Li, S. L. Mielke, G. C. Schatz, H. D. Espinosa, *Nat. Nanotechnol.*, 3, 626-631(2008).

- [17] B. Q. Wei, R. Vajtai, P. M. Ajayan, Appl. Phys. Lett., 79, 1172-1174 (2001).
- [18] E. Pop, D. Mann, Q. Wang, K. Goodson, H. Dai, *Nano Lett.*, 6, 96-100 (2006).
- [19] M. Miao, Carbon, 49, 3755-3761 (2011).
- [20] Q. Zhang, J. Q. Huang, W. Z. Qian, Y. Y. Zhang, F. Wei, Small, 9, 1237-1265 (2013).
- [21] L. Wen, F. Li, H. M. Cheng, Adv. Mater., 28, 4306-4337 (2016).
- [22] S. H. Chung, A. Manthiram, J. Phys. Chem. Lett., 5, 1978-1983 (2014).
- [23] L. Kong, H. J. Peng, J. Q. Huang, W. Zhu, G. Zhang, Z. W. Zhang, P. Y. Zhai, P. Sun, J. Xie,
 Q. Zhang, Ener. Storage Mater., 8, 153-160 (2017).
- [24] Y. C. Jeong, J. H. Kim, S. H. Kwon, J. Y. Oh, J. Park, Y. Jung, S. G. Lee, S. J. Yang, C. R. Park, *J. Mater. Chem. A*, 5, 23909-23918 (2017).
- [25] H. Yao, K. Yan, W. Li, G. Zheng, D. Kong, Z. W. Seh, V. K. Narasimhan, Z. Liang, Y. Cui, *Ener. Enviro. Sci.*, 7, 3381-3390 (2014).
- [26] S. H. Chung, A. Manthiram, Adv. Funct. Mater., 24, 5299-5306 (2014).
- [27] G. Zhou, L. Li, D. W. Wang, X. Y. Shan, S. Pei, F. Li, H. M. Cheng, *Adv. Mater.*, 27, 641-647 (2015).
- [28] L. Qie, A. Manthiram, Adv. Mater., 27, 1694-1700 (2015).
- [29] Q. Pang, J. Tang, H. Huang, X. Liang, C. Hart, K. C. Tam, L. F. Nazar, *Adv. Mater.*, 27, 6021-6028 (2015).
- [30] L. Lin, F. Pei, J. Peng, A. Fu, J. Cui, X. Fang, N. Zheng, *Nano Ener.*, 54, 50-58 (2018).
- [31] M. F. L. De Volder, S. H. Tawfick, R. H. Baughman, A. J. Hart, *Science*, 339, 535-539 (2013).
- [32]Y. P. Sun, K. Fu, Y. Lin, W. Huang, Accounts Chem. Res., 35, 1096-1104 (2002).
- [33] J. M. Bonard, H. Kind, T. Stöckli, L. O. Nilsson, Solid-State Electron., 45, 893-914 (2001).
- [34] S. Park, M. Vosguerichian, Z. Bao, *Nanoscale*, 5, 1727-1752 (2013).

- [35] Y. Ando, X. Zhao, T. Sugai, M. Kumar, *Mater. Today*, 7, 22-29 (2004).
- [36] C. Journet, P. Bernier, Appl. Phys. A-Mater. Sci. Process., 67, 1-9 (1998).
- [37] A. Szabó, C. Perri, A. Csató, G. Giordano, D. Vuono, J. B. Nagy, *Materials*, 3, 3092-3140 (2010).
- [38] M. Kumar, Y. Ando, J. Nanosci. Nanotechnol., 10, 3739-3758 (2010).
- [39] M. José-Yacamán, M. Miki-Yoshida, L. Rendon and J. G. Santiesteban, *Appl. Phys. Lett.*, 62, 657-659 (1993).
- [40] Y. Homma, T. Yamashita, P. Finnie, M. Tomita, T. Ogino, *Jpn. J. Appl. Phys.*, 41, L89-L91 (2002).
- [41] A. Oberlin, M. Endo, T. Koyama, J. Cryst. Growth, 32, 335-349 (1976).
- [42] J. W. Seo, A. Magrez, M. Milas, K. Lee, V. Lukovac, L. Forro, *J. Phys. D. Appl. Phys.*, 40, R109-R120 (2007).
- [43] Y. Wang, M. J. Kim, H. Shan, C. Kittrell, H. Fan, L. M. Ericson, W. F. Hwang, S. Arepalli, R. H. Hauge, R. E. Smalley, *Nano Lett.*, 5, 997-1002 (2005).
- [44] S. Musso, M. Zanetti, M. Giorcelli, A. Tagliaferro, L. Costa, *J. Nanosci. Nanotechnol.*, 9, 3593-3598 (2009).
- [45] M. Kumar, T. Okazaki, M. Hiramatsu, Y. Ando, Carbon 45, 1899-1904 (2007).
- [46] Z. Gao, Y. Zhang, N. Song, X. Li, *Mater. Res. Lett.*, 5, 69-88 (2017).
- [47] Z. Gao, Y. Zhang, N. Song, X. Li, *Electrochim. Acta*, 246, 507-516 (2017).
- [48] Y. Zhang, Z. Gao, X. Li, Small, 13, 1701927 (2017).
- [49] Y. Zhang, F. M. Heim, N. Song, J. L. Bartlett, X. Li, ACS Ener. Lett., 2, 2696-2705 (2017).
- [50] Z. Gao, N. Song, Y. Zhang, Y. Schwab, J. He, X. Li, ACS Sustain. Chem. Eng., 6, 11386-11396 (2018).

- [51] Y. Xie, L. Fang, H. Cheng, C. Hu, H. Zhao, J. Xu, J. Fang, X. Lu, J. Zhang, J. Mater. Chem. A, 4, 15612-15620 (2016).
- [52] G. Feng, X. Liu, Z. Wu, Y. Chen, Z. Yang, C. Wu, X. Guo, B. Zhong, W. Xiang, J. Li, J. Alloy. Compd., 817, 152723 (2020).
- [53] S. Soares, G. Camino, S. Levchik, Polym. Degrad. Stabil, 49, 275-283 (1995).
- [54] S. Costa, E. Borowiak-Palen, M. Kruszynska, A. Bachmatiuk, R. J. Kalenczuk, *Mater. Sci. Poland*, 26, 433-441 (2008).
- [55] X. Xu, C. Yang, Z. Yang, K. Yang, S. Huang, Carbon, 80, 490-495 (2014).
- [56] X. Qi, J. Xu, Q. Hu, Y. Deng, R. Xie, Y. Jiang, W. Zhong, Y. Du, Sci. Rep., 6, 28310 (2016).
- [57] Z.W. Seh, Q. Zhang, W. Li, G. Zheng, H. Yao, Y. Cui, Chem. Sci., 4, 3673-3677 (2013).
- [58] X. Qiu, Q. Hua, L. Zheng, Z. Dai, RSC Adv., 10, 5283-5293 (2020).
- [59] N. Song, Z. Gao, Y. Zhang, X. Li, Nano Ener., 58, 30-39 (2019).

Supplementary Information

Yeast-Derived Carbon Nanotube Coated Separator for High Performance Lithium-Sulfur Batteries

Jiajun He, Zan Gao, Xiaodong Li*

Department of Mechanical and Aerospace Engineering

University of Virginia

122 Engineer's Way

Charlottesville, VA 22904-4746 (USA)

*Corresponding author. E-mail: xl3p@virginia.edu, Tel: 434-243-7762

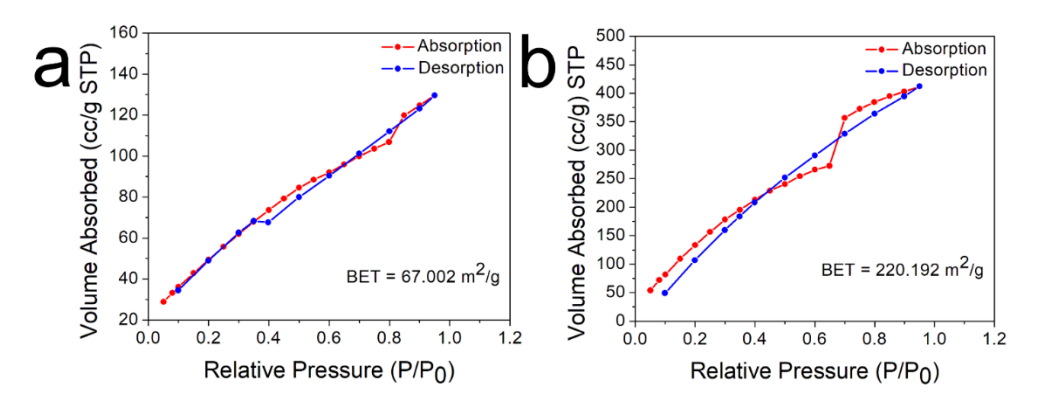


Figure S1. BET analysis of carbonized yeast and AY/CNT composite. (a) N₂ adsorption/desorption curves of carbonized yeast; (b) N₂ adsorption/desorption curves of the AY/CNT composite.

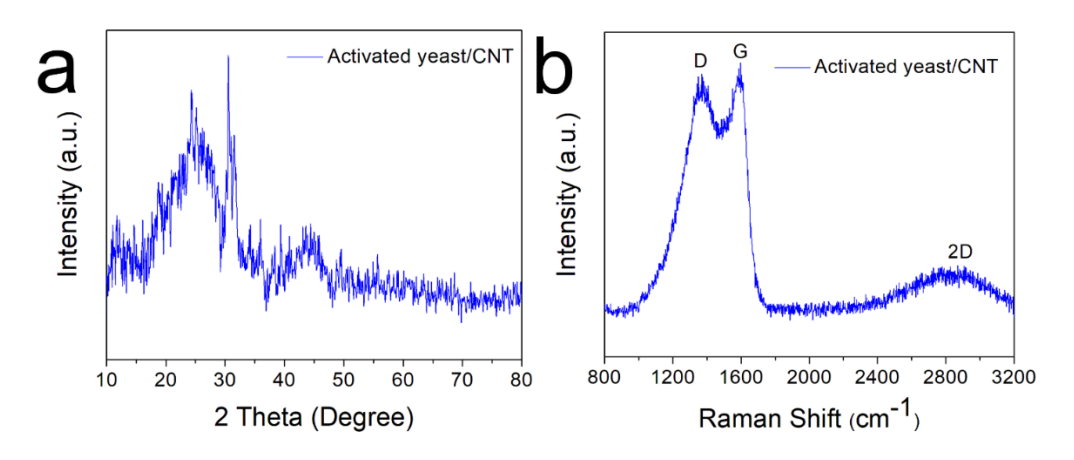


Figure S2. Characterization of the AY/CNT composite. (a). XRD spectrum of the AY/CNT composite; (b) Raman spectrum of the AY/CNT composite.

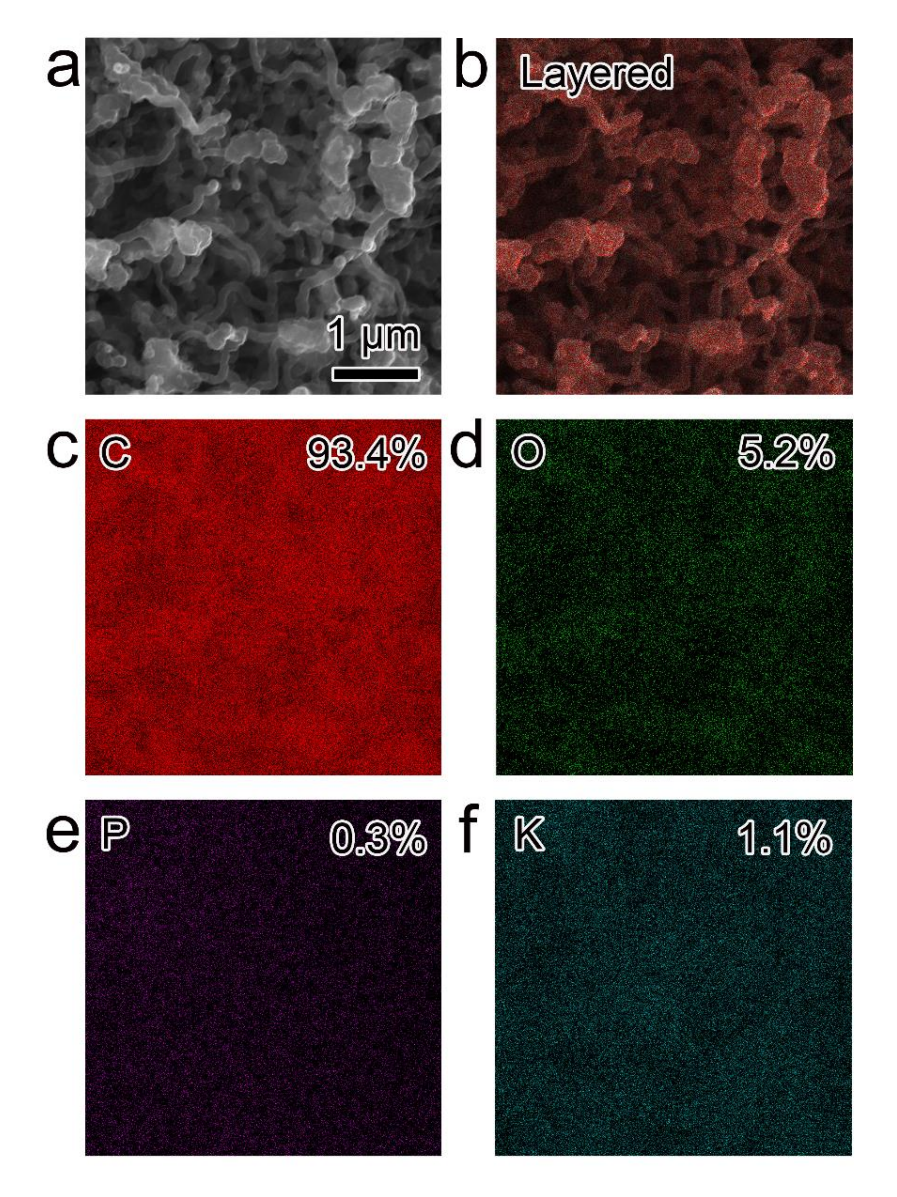


Figure S3. EDS maps of the AY/CNT composite. (a) SEM image of the AY/CNT composite; (b) Layered elemental map of the AY/CNT composite; (c-f) Element maps of C, O, P and K in the AY/CNT composite.



Figure S4. Digital image of the lithium anode from the reference battery and the battery with the AY/CNT coating after the batteries being fully discharged.

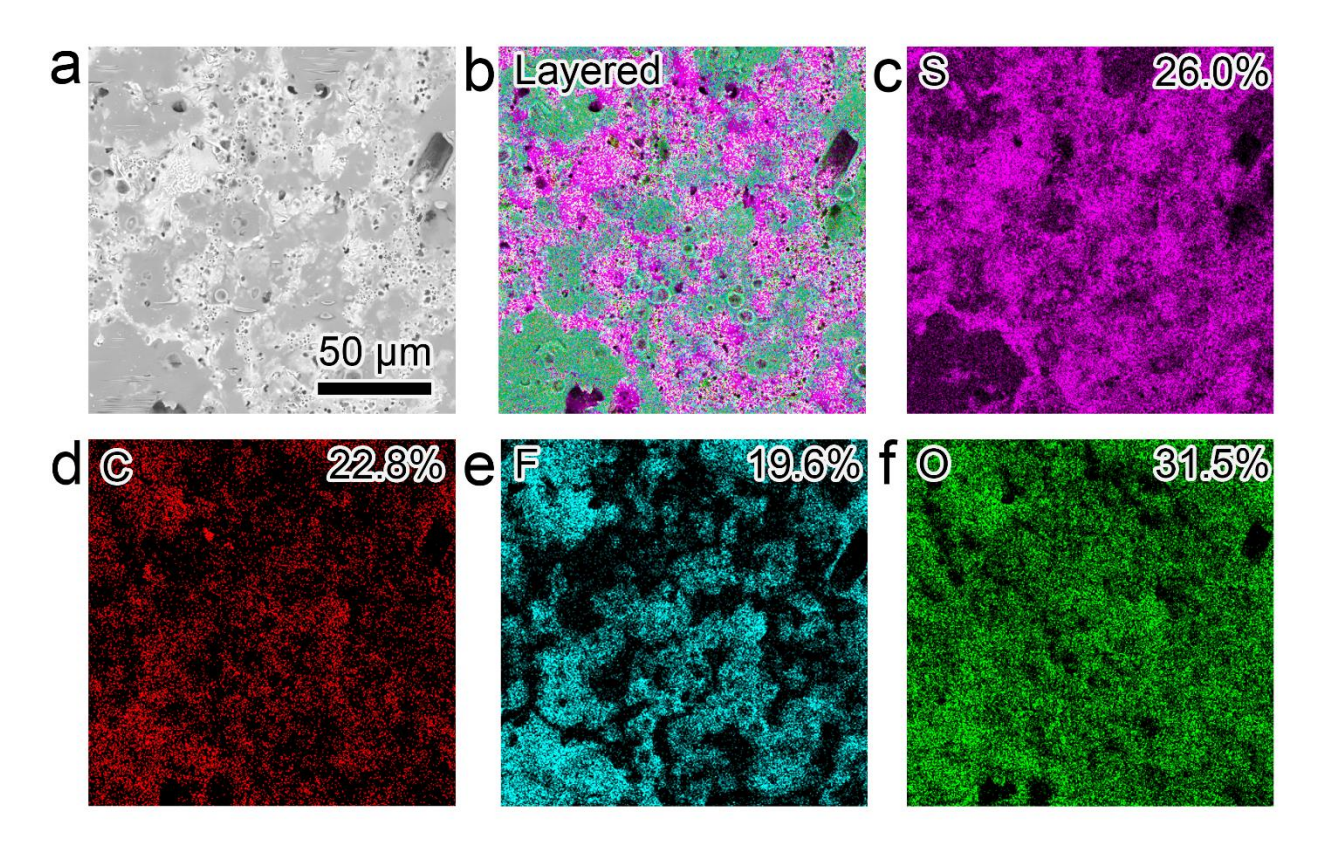


Figure S5. EDS maps of the Li anode from the reference battery after the battery was fully discharged. (a) SEM image of the anode; (b) Layered EDS map; (c-f) Element maps of S, C, F and O.

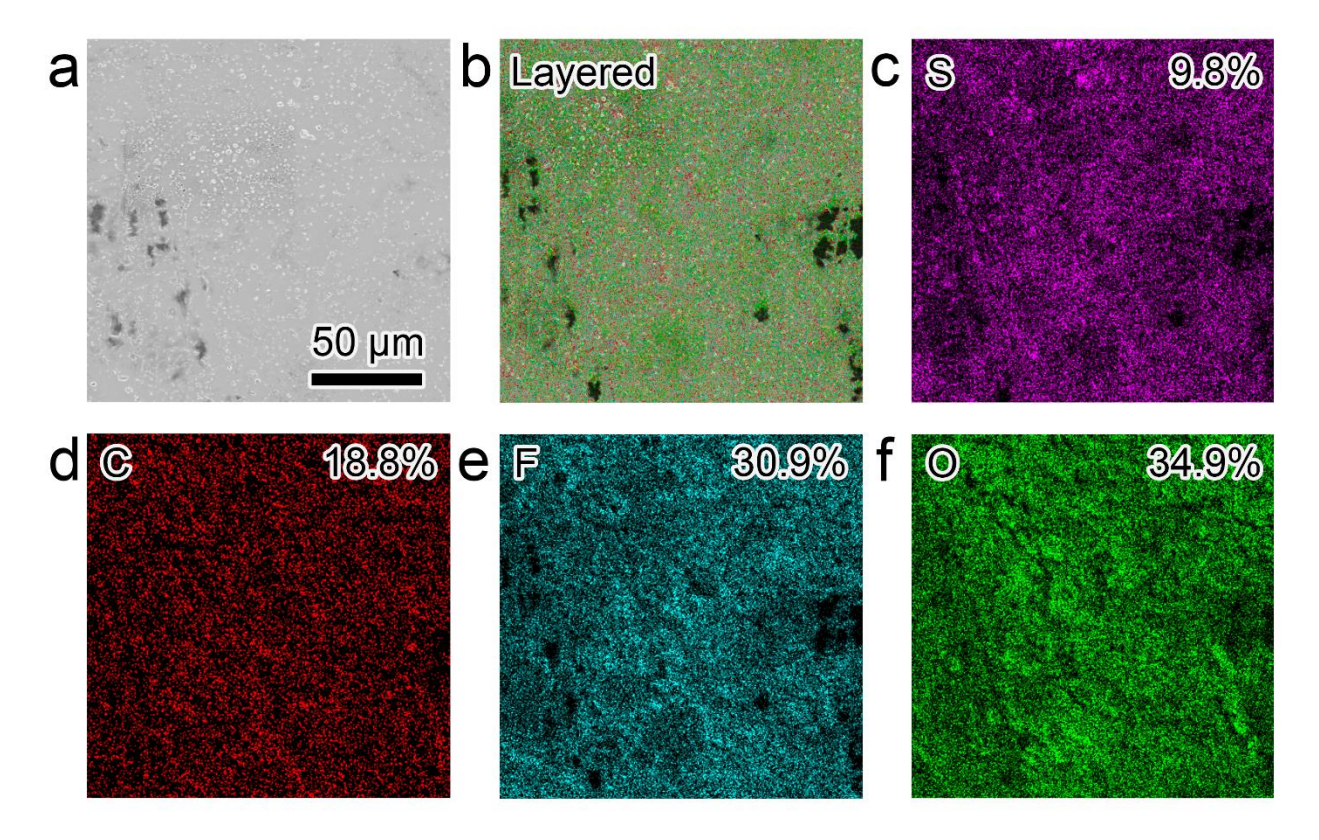


Figure S6. EDS maps of the Li anode from the battery with the AY/CNT coated separator after the battery was fully discharged. (a) SEM image of the anode; (b) Layered EDS map; (c-f) Element maps of S, C, F and O.

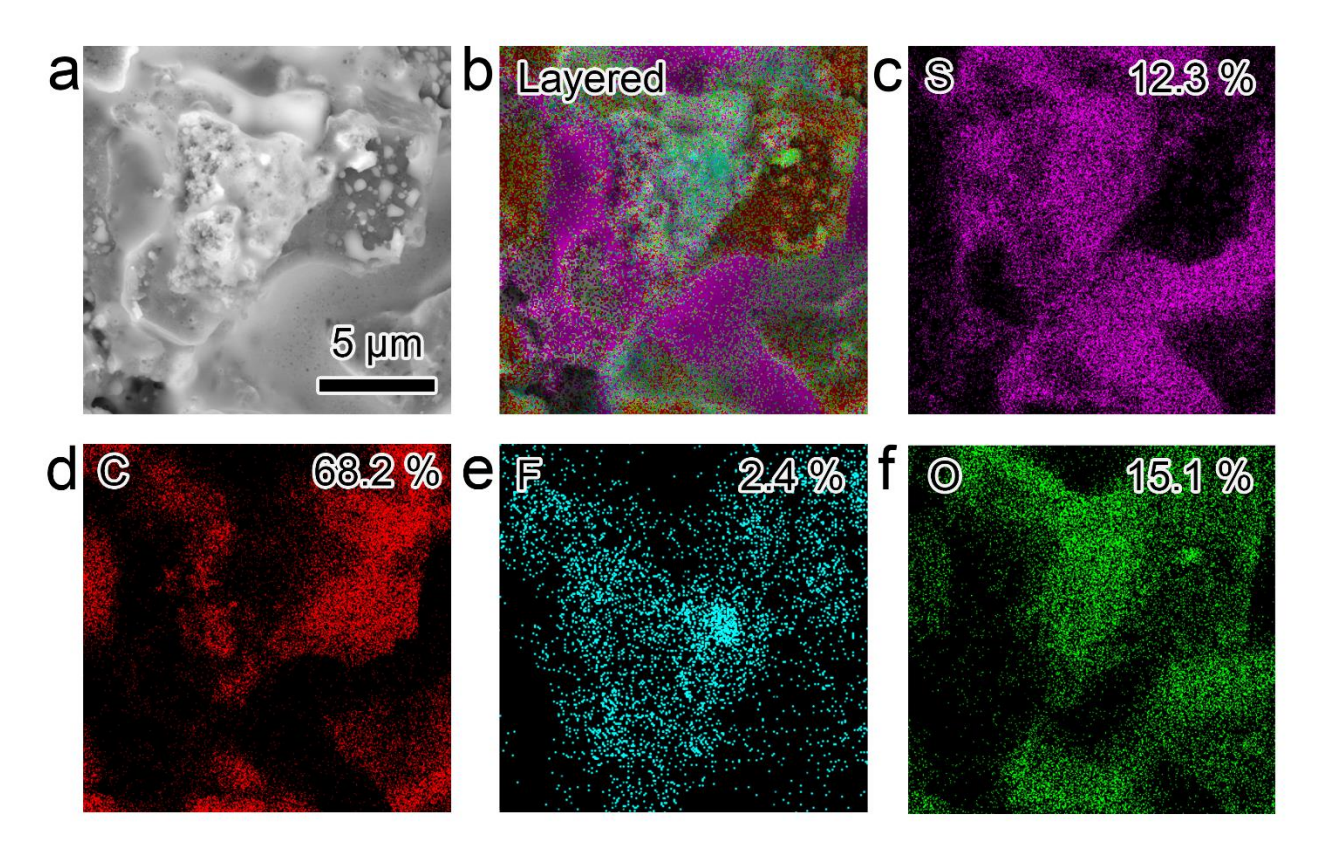


Figure S7. EDS maps of the AY/CNT coating after the battery was fully discharged. (a) SEM image of the AY/CNT coating; (b) Layered EDS map; (c-f) Element maps of S, C, F and O.

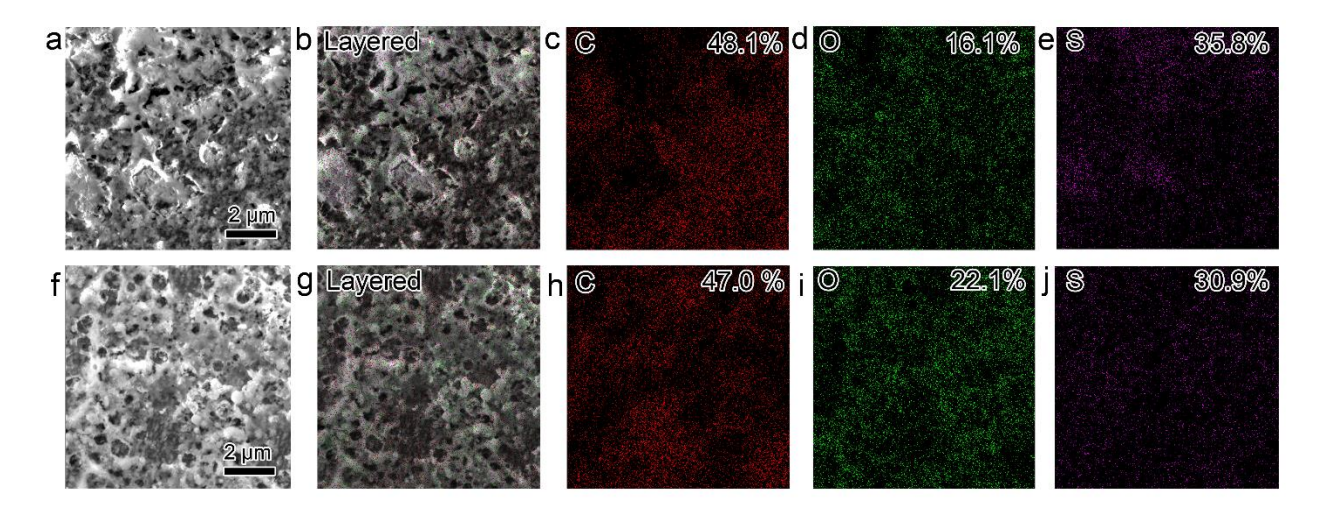


Figure S8. EDS maps of the separator from the reference battery after the battery was fully discharged. (a-e) EDS maps of the cathode side of the reference separator; (f-j) EDS maps of the anode side of the reference separator.